Analysis of Ion Transport in Nanofiltration Using Phenomenological Coefficients and Structural Characteristics

Sarit Bason, Yair Kaufman, and Viatcheslav Freger*

Zuckerberg Institute for Water Research and Department of Biotechnology and Environmental Engineering, Ben-Gurion University of the Negev, Sde-Boqer, 84990 Israel

Received: September 1, 2009; Revised Manuscript Received: January 19, 2010

The analysis of salt transport in nanofiltration using extended Nernst−Planck equations or similar models often suffers from the difficulties to establish and independently and transparently verify the consistency between the filtration results, assumed mechanism, and fitted values of parameters. As a general alternative, we propose here a procedure that reduces filtration data to two general phenomenological coefficients, concentration-dependent salt permeability ω_s and Peclét coefficient A, which does not require that a specific exclusion mechanism be assumed and thus allows a transparent test on consistency with commonly used models. This approach was demonstrated using concentration polarization-corrected filtration data for NF-200 membrane and four monovalent salts, NaCl, NaBr, KBr, and KCl. The coefficient A was found to be very small, which points to the negligible contribution of convection to salt transport. The smallness of A was verified through estimates of the effective pore radius of the membrane, found to be between 0.2 and 0.3 nm, and comparing them with similar independent estimates from the hydraulic permeability L_p using the data on the thickness and swelling of the selective polyamide layer obtained by AFM. The concentration dependence of ω_s and its variation for different salts suggested that in the concentration range above 0.01 M the salt exclusion may be dominated by a combination of Donnan and dielectric mechanisms. The values of ω_s obtained for single salts were also consistent with the selectivity observed for equimolar feed mixtures of NaCl and NaBr. However, the observed variation of ω_s with concentrations of single salts below 0.01 M reveals a new regime that is inconsistent with all commonly used models of NF based on a Donnan mechanism modified with dielectric and steric effects. In particular, ω_s appeared to approach a constant value at low salt concentrations, whereas the standard mechanisms predict a linear or even steeper decrease as concentration decreases. This puzzling discrepancy could have passed unnoticed in the standard multiparameter fitting extended Nernst−Planck equations and demonstrates the benefits of the present phenomenological analysis.

1. Introduction

Nanofiltration (NF) is often used for ion separations, taking advantage of different selectivities toward various ion and higher fluxes than in reverse osmosis (RO). Presently, the accepted framework for physical modeling of NF is the extended Nernst−Planck (ENP) differential equations for each ion coupled with two electroneutrality conditions for ion fluxes and local concentrations.[1−9] In the case of a single salt these reduce to the classic Spiegler−Kedem (SK) equation for the salt.[10] However, these fundamental equations are only frameworks and contain *coefficients* that must be calculated using appropriate thermodynamic and kinetic models of ion exclusion and transport within the active layer. Such calculations critically depend on (1) assumptions regarding the exclusion mechanism and (2) the physical characteristics of the membrane and ions, such as pore size, fixed charge, and dielectric properties of the membrane and size and charge of ions involved. Virtually all published models of NF relied on certain relations based on the hindered transport theory[11,12] and on three ion exclusion mechanisms, steric, dielectric, and Donnan (electric) (SDE),[1,2,13] sometimes with the addition of specific interactions with the polymer of the active layer.[14]

The nearly unanimous reliance on the regular SDE relations that are usually "plugged" into ENP equations has never been critically examined and systematically compared with what the experiments actually show. An important factor was the difficulty to measure characteristics of the very thin and nonuniform active layer. For this reason questionable multiparameters fitting of flux-rejection data to the above equations (tacitly assumed correct) was the main source of information with limited ability to independently validate the deduced characteristics. Some progress was recently achieved in developing methods for measuring physical characteristics of the thin active layer.[15,16] However, a transparent data analysis that would put the common assumptions under scrutiny in a model-independent way has been missing.

Recently, we proposed a new phenomenological approach that may fill the large gap between the experimental data and physical modeling for the single salt case.[17,18] An important earlier work exploring a similar approach was done by Yaroshchuk.[19] It is based on general relations between phenomenological coefficients of the SK model, the salt permeability ω_s, and either the reflection coefficient σ_s or the Peclét coefficient $A = (1 - \sigma_s)/\omega_s$. Importantly, coefficient A should be weakly dependent on salt concentration in most circumstances, whereas the other two should be concentration-dependent. Thus, by adopting A and ω_s as the set of coefficients, the concentration dependence of ω_s may be directly deduced from flux-rejection

* To whom correspondence should be addressed. E-mail: vfreger@bgu.ac.il.

10.1021/jp911615n
Published on Web 02/19/2010

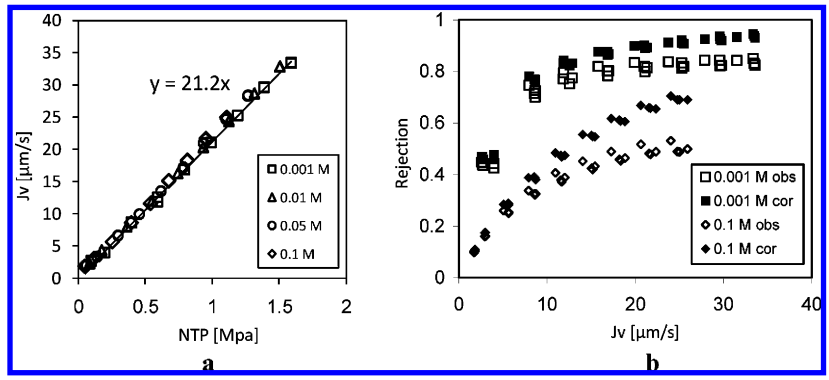

Figure 1. Filtration results for KCl solutions of different concentrations using NF-200 membranes: (a) volume flux vs net transmembrane pressure for several different feed concentrations; (b) KCl rejection, observed (open symbols) and corrected (filled symbols), vs volume flux for two different feed concentrations, 0.001 (squares) and 0.1 M (diamonds).

data without the need to consider specific mechanisms. The SK equation is then written in the following form:

$$\frac{dc}{d\bar{x}} = AJ_V\left[c - \frac{c''}{A\omega_s}\right] \quad (1)$$

where c is the local corresponding concentration, c'' the permeate concentration, and $0 \le \bar{x} \le 1$ is the distance from the feed side scaled to the total membrane thickness. The concentration-dependent ω_s in eq 1 has a transparent relation to exclusion mechanism; in particular, when compared for different salts, it may serve as a fingerprint for distinguishing between different mechanisms and estimating some important characteristics of the membrane and solutes.

In this paper we implement this approach for analyzing the phenomenological coefficients A and concentration-dependent ω_s for several monovalent salts and NF-200 membrane in conjunctions with some independently measured structural characteristics of the membrane. Our main purpose is to *examine the validity of the common relations of ion exclusion*, which will be shown to fail in a certain concentration range. However, the utility of this approach and wealth of information directly extractable from the coefficients will also be demonstrated in other ways. Finally, we will briefly consider the question of applicability of the obtained coefficients for single salts to salt mixtures, which is the crucial step toward predictive modeling of NF.

2. Materials and Methods

2.1. Filtration Experiments. The NF-200 membrane (Dow-Filmtec) and feed solutions of single monovalent salts NaCl, NaBr, KBr, KCl (all analytical grade), and mixed solutions of NaCl and NaBr in 1:1 molar ratio were used in filtration experiments. The setup is fully described elsewhere.[18,20] Briefly, two flat channel flow cells of wet membrane area of 17.6 cm^2 mounted in series were used in each experiment for duplicate tests. The solution from a pressurized feed tank (1.5 L) was circulated through a thermostat that maintained a constant temperature of 25 °C in the cells back to the tank by means of a gear pump. In all experiments except those used to determine mass-transfer coefficients the average fluid velocity was 0.47 m/s on the basis of the channel cross-section of 22 × 2 mm^2.

The volume flux J_V was determined by collecting and weighing the permeate over a certain time, and observed rejections R for single salts were determined by measuring the conductivity of feed, retentate, and permeate. The feed and permeate were in the range of pH 6.5−7. The concentrations of halide ions (Cl^- and Br^-) in experiments with salt mixtures were determined using a 4500i ion chromatograph with an AS4A-SC column (Dionex). The hydraulic permeability coefficients L_p were determined for each salt and feed as the slope of flux plotted versus net transmembrane pressure (NTP). The latter was the difference between the gauge pressure and the osmotic pressures difference between feed (corrected for concentration polarization—see next paragraph) and permeate calculated using OLI software (OLI System, Inc.). Figure 1a exemplifies results for KCl and the full data for all salts are presented in the Supporting Information (Figure S1). For all solutions, the pressure was varied between about 0.2 and 2 MPa and all obtained L_p were in the range of 20.2−22.6 μm/(s·MPa) (7.3−8.1 L/(m^2·h·bar)), which within the error margin was similar to the value for pure water 21.0 μm/(s·MPa) (7.6 L/(m^2·h·bar)) and to the manufacturer's value of 21.4 μm/(s·MPa) (7.7 L/(m^2·h·bar)).[21]

Prior to model fitting, the observed feed concentrations c_F and observed rejections $R_{obs} = 1 - c''/c_F$ were corrected for concentration polarization.[18] In contrast to many previous studies on NF,[5,22−24] such correction was found to be crucial for meaningful data analysis. The corrected feed concentration c' was obtained using the relation

$$c' = (c_F - c'')\exp\left(\frac{J_V}{k_d}\right) + c'' \quad (2)$$

yielding the corrected rejections $R = 1 - c''/c'$. The mass-transfer coefficient k_d was determined from separate experiments by varying the cross-flow velocity in the channel v. A relation for undeveloped laminar flow $k_d = \kappa v^{1/2}$ was used, where κ is a constant of dimensions $(m/s)^{0.5}$ determined by channel geometry and physicochemical properties of the fluid and solute (see Supporting Information);[25,26] thereby R_{obs} varies as follows

$$\ln\left(\frac{1 - R_{obs}}{R_{obs}}\right) = \ln\left(\frac{1 - R}{R}\right) - \frac{J_V}{\kappa v^{1/2}} \quad (3)$$

The parameter κ was determined from nine series of duplicate experiments with different salts. Since for given hydrodynamic conditions κ is proportional to $D^{2/3}$, where D is the diffusion coefficient of the salt,[25,26] to combine data for all salts "normalized" parameters $\kappa^* = \kappa/D^{2/3}$ were actually calculated from plots of $\ln[(1 - R_{obs})/R_{obs}]$ versus $J_V/v^{1/2}D^{2/3}$ and averaged for all experiments. Ultimately, mass-transfer coefficients for correcting rejection for each salt were calculated as $k_d = v^{1/2}D^{2/3}\kappa^*$ using

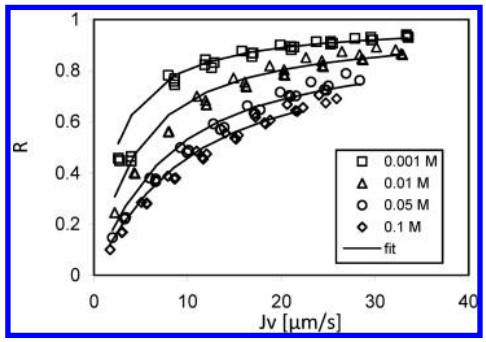

Figure 2. Corrected rejections vs volume fluxes for NF-200 and KCl. The solid lines are the best fits using eq 1 and eq 4.

$v = 0.47$ m/s. The details may be found in the Supporting Information (Table S1 and Figures S2 and S3), and an example of obtained and corrected rejections is shown in Figure 1b.

It must be stressed that k_d actually varies (decreases) along the channel.[25] As a result, the observed c'' was the average over the whole surface, since c', c'', and R all vary through variations of k_d and ω_s, even though c_F stays nearly constant. Our analysis[27] shows however that, for the hydrodynamic conditions, polarization levels, and $\omega_s(c)$ obtained in this work, the use of single (averaged) k_d, c', and R results in c' that differs by no more than 10% from the value that would be obtained for given c_F and c'', were the mass-transfer conditions truly uniform. Such an error apparently justifies the use of an average k_d.

2.3. Determination of Coefficients *A* and ω_s. The fitting algorithm was fully explained and described in our previous publications.[17,18] Briefly, all data for several feeds containing the same single salt were simultaneously fitted to eq 1. For a given salt, the Péclet coefficient A was assumed to be a constant[17] and ω_s was assumed to vary with c following the relation

$$\omega_s = a_1 c^{a_2} + a_3 \tag{4}$$

where a_1, a_2, and a_3 are fitting parameters. Equation 4 with $a_3 = 0$ was used previously by Yaroshchuk[19] as it is compatible with the regular SDE mechanism in the considered concentration range. However, addition of a finite free term a_3 was crucial for addressing some unexpected features in the low concentration range (see section 3.1). An example of fitted rejection data for KCl in Figure 2 shows that reasonable fits could be produced using eq 1 and eq 4. (Results for all salts are presented in the Supporting Information, Figure S4.)

2.4. Membrane Thickness and Swelling Using AFM. The thickness and equilibrium water content of the active layer of NF-200 were measured using an atomic force microscopy (AFM) based method reported previously.[28] Since pore size calculations are sensitive to these characteristics, the previous estimates were verified and corrected.

The polyester nonwoven backing was carefully peeled off the membrane. A small piece of a silicon wafer was dipped in *N*,*N*-dimethylformamide (DMF) and, while wet, used to gently touch the polyamide side of the membrane so that the membrane stuck to the silicon surface. DMF was then poured onto the sample dropwise to slowly dissolve and wash away the polysulfone layer to obtain a free polyamide layer firmly attached to the silicon wafer. Then, the isolated polyamide was immersed for several minutes in pure DMF for final cleaning and removal of polysulfone residues. Finally, the sample was repeatedly scratched with a sharp needle to form narrow strips of polyamide on a hard and flat Si surface.

Samples were imaged by AFM using a Nanoscope 3D Multimode (Veeco) microscope keeping the temperature of the stage and sample at 25 °C using temperature control. NP-S cantilevers with 0.12 N/m spring constant (Veeco) were used in contact mode. The cantilever deflection was set to keep the repulsive force constant for all scans (13 ± 2 nN). This relatively high repulsive force ruled out electrostatic interactions and ensured hard-core steric repulsion between the tip and the sample surface.[28] Strips were first imaged in dry state (in ambient air at 25 °C) taking care to have bare Si on both sides of the strip. Then, the sample was covered with distilled water, 60 min were allowed for equilibration, and the same area was scanned again. The images were flattened using a second-order correction; flattening being applied only to the bare substrate areas on both sides of the film, excluding the area occupied by the film. For thus flattened film the average thickness was determined using the built-in manufacturer's software as the distance between the two dominant peaks in the depth histogram corresponding to the bare Si substrate and film areas, respectively, as illustrated in Figure 3. The results were averaged over five different samples. The water volume fraction in the films ϕ was determined from the wet and dry polyamide thickness Δx as

$$\phi = (\Delta x_{wet} - \Delta x_{dry})/\Delta x_{wet} \tag{5}$$

3. Results and Discussions

3.1. Deduced Concentration Dependence of ω_s for Different Salts. The fitted concentration dependence of $\omega_s(c)$ for all measured salts is summarized in Figure 4. It is seen that for all univalent salts the obtained trends are similar. Note that the use of eq 4 was not critical, and insignificant differences were obtained using other equations that could adequately fit the concentration dependence of ω_s. This concentration dependence $\omega_s(c)$ shown in Figure 4 could then be reproducibly obtained; this dependence (rather than the particular values of a_1, a_2, and a_3 in Table 1) may well be viewed as a robust *experimental result*. As such, it could be subsequently analyzed for consistency with any specific rejection mechanism.

The most striking feature of the obtained $\omega_s(c)$ is a finite value approached at low concentrations (i.e., a nonzero a_3) clearly seen in Figure 4 for all salts except KBr. No reasonable fits could be produced for a_3 set to zero (which was the main reason for the particular choice of eq 4). Regardless of the physical reason, such behavior at low concentrations is *fundamentally inconsistent* with the commonly used relations describing the SDE exclusion as explained in section 3.3. However, at higher concentrations the permeability increases somewhat slower yet qualitatively similar to what the existing models predict. The smaller than theoretical slope in this range was already noted by Yaroshchuk,[19] who analyzed a more narrow concentration range (0.01−0.1 M) and suggested that incomplete dissociation and inhomogeneous fixed charge density could be likely causes. By extending the range in this study to lower concentration, another exclusion regime incompatible with the regular SDE picture was made apparent; the lower slope may then well result from a slow crossover to this low-concentration regime.

Another notable point analyzed in the next section and already mentioned in previous publications (see also ref 29) was that the fitted values of A were very low, in the range of (2.1−2.7)

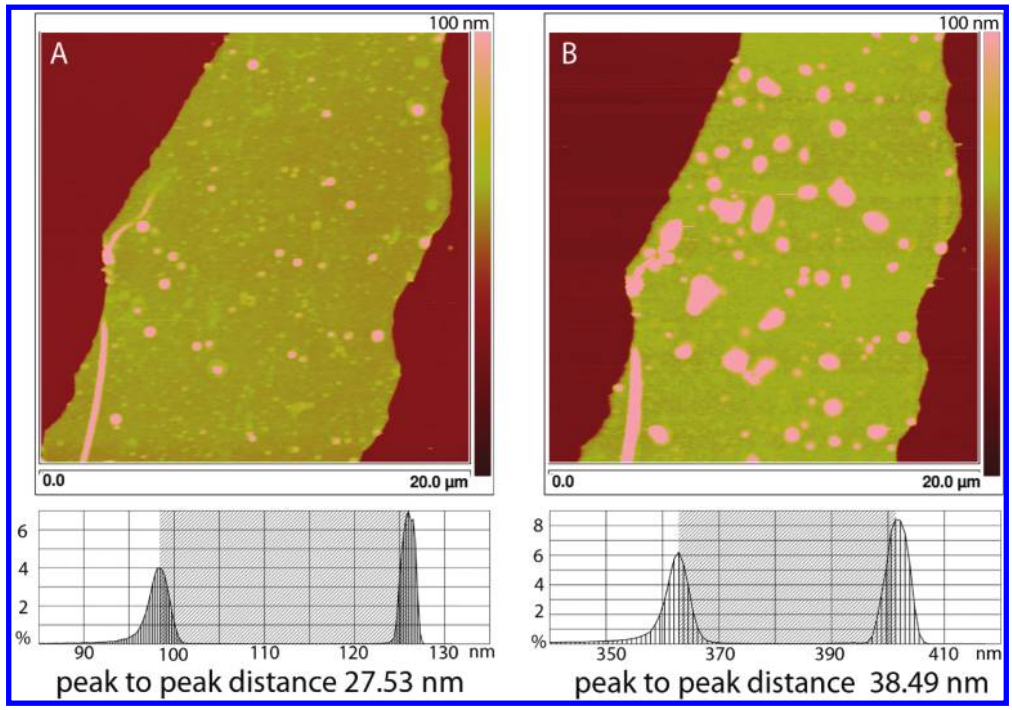

Figure 3. Flattened AFM topography images of NF-200 active layer on a Si wafer: (A) dry; (B) after 60 min in DI water. The two peaks in the histograms shown under the images correspond to the heights of the film and bare Si substrate; the difference between the heights is taken as the polyamide thickness.

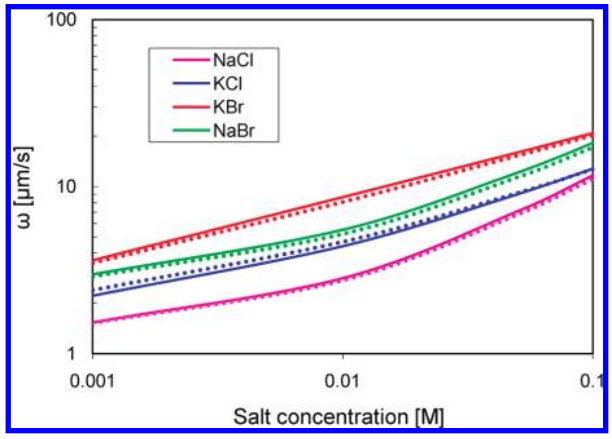

Figure 4. Concentration dependence of salt permeability ω_s for NaCl, NaBr, KBr, and KCl deduced from experimental data. The solid and dotted lines designate fits to, respectively, eq 1 and eq 6 using in both cases eq 4 for $\omega_s(c)$.

$\times 10^3$ s/m ($(5.9-7.3) \times 10^{-4}$ L^{-1}·m^2·h) for all salts, as shown in Table 1. These low values are a direct consequence of the very small thickness of the active layer. For practical purposes this means that the term containing A may be dropped and eq 1 may be simplified to become

$$\frac{dc}{dx} \approx -J_V c'' \frac{\sigma_s}{\omega_s} \approx -J_V c'' \frac{1}{\omega_s} \tag{6}$$

where the last equality also uses the smallness of $1 - \sigma_s = A\omega_s$. When eq 6 with only three parameters defined by eq 4 was used in place of eq 1, the obtained $\omega_s(c)$, also presented in Figure 4 as dotted lines, showed only marginal differences with the full four-parameter fit including A as well. This conclusion is in full agreement with Yaroshchuk et al.,[30] who recently presented evidence of negligible contribution of convection in thin-film NF composites, i.e., in our terms, the smallness of A and validity of eq 6. However, the fitted values of A were much less certain than $\omega_s(c)$, since the fits were weakly sensitive to the value of A. This means the smallness of A, critical for using eq 6, needed to be independently verified. One possible way is presented in the next section.

3.2. Smallness of A and Consistency with L_p Verified through Effective Pore Size and AFM Data. A possible way to corroborate the smallness of the Péclet coefficient A is to examine its consistency with another coefficient, the hydraulic permeability L_p, that is determined with good accuracy. Both coefficients are purely frictional and may be related to and produce consistent estimates of the effective pore radius r_p, a parameter of great interest in NF. Of course, the dense active layer has no permanent pores in the usual sense; however, water and solutes traveling through this swollen polymer network experience frictional forces that *may* be adequately related to an effective mesh or pore size, as argued below. Nevertheless, we stress that the present calculations are mostly meant to verify the smallness of A, rather than supply estimates of r_p.

The suitable expressions for A are as follows[17]

$$A = \Delta x \frac{\alpha(\phi)}{\phi} \frac{f_{sw}}{nRT} = \Delta x \frac{\alpha(\phi)}{\phi} \frac{6\pi\mu}{k_B T} \left(r_1 \frac{K_c(\lambda_1)}{K_d(\lambda_1)} + r_2 \frac{K_c(\lambda_2)}{K_d(\lambda_2)} \right) \tag{7}$$

where f_{sw} is the salt-water friction coefficient, which is the sum of the friction coefficients of anion and cation with water, α the tortuosity factor, Δx the membrane thickness, μ the effective viscosity of water, and $n = 2$ for a monovalent salt. The first equality is actually the rigorous phenomenological relation, whereas in the second the term f_{sw}/nRT is replaced with the sum of contributions by anion (1) and cation (2) expressed as the product of the "unhindered" Stokes−Einstein term $6\pi\mu r/k_B T$ and a hindrance factor $K_c(\lambda)/K_d(\lambda)$ depending on the ratio

TABLE 1: Fitted Parameters a_1, a_2, and a_3 (Equation 4), A, and L_p for NF-200 and Different Salts and Estimates of the Effective Pore Radius r_p from A using the Stokes and Pauling Ionic Radii and from L_p

salt	$A \times 10^{-3}$ (m^{-1} s)	a_1[a]	a_2[a]	a_3[a]	r_p[b] (nm)	r_p[c] (nm)	L_p ($\mu m \cdot s^{-1} \cdot MPa^{-1}$)	$r_p(L_p)$ (nm)
NaCl	2.17	67.1	0.836	1.31	0.282	0.294	22.6	0.217
NaBr	2.43	76.7	0.714	2.34	0.301	0.284	21.4	0.214
KCl	2.65	39.6	0.548	1.50	0.277	0.191	21.2	0.211
KBr	2.13	51.6	0.423	0.70	0.322	0.200	20.2	0.212

[a] Coefficients of eq 4 for c in moles per liter and ω_s in micrometers per second in the range of 0.001 M $\leq c \leq$ 0.1 M. [b] Based on the Pauling ionic radii. [c] Based on the Stokes ionic radii for r_s.

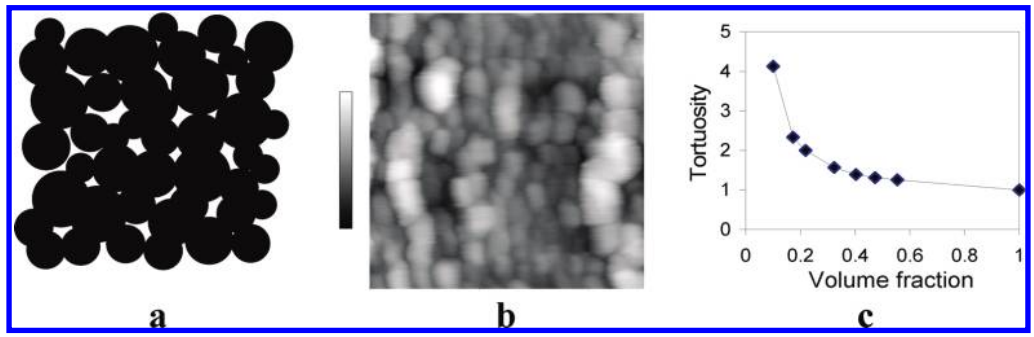

Figure 5. (a) Assumed geometry of the membrane. (b) AFM topographic image of the NF-200 surface: image size, 1 × 1 μm^2; vertical color scale, 50 nm; after ref 43. (c) Effective tortuosity of random composites composed of overlapping spheres: after Torquato et al.[31]

of ion and pore radii $\lambda = r/r_p$. The functions K_c and K_d were introduced in the hindered transport theory[11,12] and express, respectively, the convective and diffusive hindrance.

An analogous general relation for L_p is[31,32]

$$L_p = \frac{b r_p^{\,2}}{\mu \Delta x} \frac{\phi}{\alpha} \tag{8}$$

where b is a geometric parameter that may vary by about on order of magnitude depending on the pore geometry.[33] Equations 7 and 8 imply a "macroscopic" view on the molecular friction that involves an effective viscosity, which might be justly criticized as a questionable and even inadequate concept for transport in nanopores. Nevertheless, some observations suggest that the associated error is probably not large. First, there have been numerous indications that diffusion and convection of solvents within homogeneous polymer solutions and gels are reduced relative to bulk solvent in a fairly universal manner at least down to solvent volume fractions of 10−20%.[28,34−37] This trend suggests that, within this range (covering water content in NF membrane), the solvent mobility is mostly effected by geometric and nonspecific obstruction by polymer rather than through reduced microscopic mobility (viscosity), even through polymer and solvent interact at the molecular (sub-nanometer) scales. Recently, direct mechanical measurements on confined water layers indicated that water exhibits nearly bulklike viscosity in confined layers at least down to a monolayer thickness, from which one concludes no drastic viscosity correction is required for water in nanopores.[38,39] The last and probably most important observation is that eqs 7 and 8 are affected by the uncertainties in viscosity (as well as tortuosity, porosity, and film thickness) in a similar manner; therefore deviation of viscosity from its bulk value should similarly, though perhaps not identically, affect both pore size estimates, from L_p and A.

We updated here the past AFM results[28] to obtain the membrane thickness $\Delta x = \Delta x_{wet} = 35 \pm 6$ nm and porosity $\phi = 0.26 \pm 0.04$, the errors being standard deviations. To calculate the tortuosity that in general depends on porosity and microstructure,[40] we approximate the polymer structure with a 3D random array of multisized overlapping spheres (Figure 5a). Unlike the often used model of straight pores, this model seems to suit best the observed morphology of the active polyamide layer (cf. Figure 5b) and current understanding of its formation, which proceeds as aggregation of growing spherical particles.[41,42] This model was extensively studied by simulations, and the resulting dependence $\alpha(\phi)$ displayed in Figure 5c appears to be representative of a wide class of random porous media.[31,32] Using this result we could estimate that $\alpha \approx 1.8$ for $\phi = 0.26$. Simulations also show that the value $b = 1/8$ produces a reasonable estimate for such systems.[33] This value of b is reminiscent of the Hagen−Poiseuille equation, yet eq 8 is essentially different from the latter in that it contains tortuosity and implies a random pore structure.

The assumed microstructural model implies a fairly wide distribution of pore resistances within the random pore network, which is believed to be a common property of many random composites.[32,44] Given this feature, r_p in both equations assumes the meaning of the critical pore radius, i.e., the smallest pore of the subset of larger, less resistant, pores just forming an infinite percolating subnetwork within the whole pore network.[31] Since eqs 7 and 8 both involve a strong dependence on r_p (through $K_c(\lambda)/K_d(\lambda)$ and r_p^2), such a critical "bottleneck" pore determining the overall permeability will be about the same sharply defined size both for water and solute transport. This means the difference between estimates of r_p from L_p and A must be fairly small, regardless of the effective value of viscosity, provided the two coefficients are consistent. Of course, this will be true within the ambiguity of the ionic radii (see Table 2) that "converts" the critical λ to critical r_p in the case of A.

Calculations of r_p based on the values of L_p and A and eqs 7 and 8 are summarized in Table 1. In the case of A separate estimates were made using Stokes and Pauling (bare) radii (see Table 2). The Stokes radii exactly reflect frictions of hydrated ions in bulk water; however, inside the membrane the ions may be partly stripped of hydration shells and experience a different friction, which is why the Pauling radii represent another limiting case. Table 1 shows that both L_p and A produce close values of

TABLE 2: Stokes, Pauling, and Born Radii (nm) of Ions Involved

ion	Stokes[a]	Pauling[45]	Born[46]
Na^+	0.184	0.098	0.169
Cl^-	0.121	0.181	0.202
K^+	0.125	0.133	0.200
Br^-	0.118	0.196	0.219

[a] Calculated from ion diffusivities in water.[47]

pore radius, those obtained from L_p, around 0.21 nm, being slightly lower than the values between 0.2 and 0.3 nm obtained from A using the Stokes and Pauling radii. A possible reason for discrepancies pointed out by an unknown reviewer could be the resistance of the support layer that affects L_p but not A. However, the discrepancies seem to be reasonable in view of the crudeness of the model and uncertainties of the values of A and ionic radii. The plausible values of pore radius suggest that A is indeed close to our estimates and is very small. This means the practical use of a simplified eq 6 is well-justified.

We note that our crude estimates are smaller than some earlier estimates for this and similar piperazine−amide NF membranes, which are closer to 0.4−0.5 nm.[23,48,49] The latter were mostly obtained from filtration of neutral hydrophilic solutes and inorganic ions as size-exclusion probes. However, the rejection of such solutes could be affected by the partitioning factor K (see next section) that may depend on solute size in a more complex and often opposite manner than frictions.[50] On the other hand, neither A nor L_p contain K; hence the present estimates were free of such effects.

3.3. Concentration Dependence of Salt Permeabilities and Its Interpretation. The permeability of a univalent salt is related to the friction and partitioning coefficients through the relation[17]

$$\omega_s = \frac{2RTK}{\Delta x\left(f_1\frac{Kc}{X+Kc}+f_2\right)} \approx \frac{2RT}{f_2\Delta x}K \qquad (9)$$

where K is the partitioning coefficient of the co-ions or, identically, the free salt invading the membrane, X is the fixed charge density, and f_1 and f_2 are the friction coefficients that sum up the frictions with water and membrane of counter- and co-ions, respectively. The last approximate expression holds when $c \ll X/K$, i.e, when the fixed charge exceeds the invading salt, which apparently holds for the analyzed concentration range, as explained below. Since the frictional factors negligibly vary with concentration, as the nearly constant values of L_p suggest (see Figure 1a and Table 1), the dependence of ω_s on concentration and, to a large extent, on salt type mostly comes from the salt partitioning coefficient K.

The observed trend in intermediate and upper concentration ranges may be rationalized using a simple SDE model put forward by Yaroshchuk et al.[51] that calculates K as a combination of Donnan and non-Donnan contributions. The non-Donnan part is described by a constant non-Donnan partitioning coefficient K_0. This results in an expression

$$K = -\frac{X}{2c} + \sqrt{\frac{X^2}{4c^2} + {K_0}^2} \qquad (10)$$

Its limiting behavior at high and low c is

$$K \approx K_0 \quad \text{for } c \gg X/2K_0 \qquad (11a)$$

$$K \approx \frac{{K_0}^2 c}{X} \quad \text{for } c \ll X/2K_0 \qquad (11b)$$

For a 1:1 salt the coefficient K_0 is related to the non-Donnan partitioning coefficients, i.e., affinities toward the membrane, of cation k_0^+ and anion k_0^- as follows

$$K_0 = (k_0^+ k_0^-)^{1/2} \qquad (12)$$

Note that the partitioning coefficient K in eqs 10 and 11 is that of the co-ions, yet eq 12 shows that the affinities of co- and counterion both affect K.

The effect of cations and anions on the salt permeability is clearly seen in Figure 4, particularly, in the intermediate and upper concentration ranges, i.e., 0.01−0.1 M. Every replacement of Na^+ with K^+ and Cl^- with Br^- for a given c seems to increase the salt permeability by some factor, in full agreement with eq 12. This is more explicitly seen in Figure 6 showing the ratios of permeabilities for different salt pairs with a common ion. Interestingly, the permeability appears to be larger for salts composed of cations and anions with *larger* Pauling or Born radii (Table 2), as predicted by the Born equation in agreement with previous reports.[18,52] The larger permeability of larger ions points to a dominant contribution of the dielectric exclusion to the parameters K_0 for salts and k_0 for ions rather than steric effects (the latter would result in a larger permeability of smaller ions) in the range of $c > 0.01$ M.

Figure 4 indicates that the salt permeability ω_s steadily increases with concentration, as characteristic of the regime $c \ll X/2K_0$; therefore the approximation of fixed charge far exceeding the invaded free salt may be reasonable in the whole c range. On the other hand, it is also seen that in the upper concentration range the differences between different salts decrease, i.e., the ratios become closer to 1, which is consistent with eqs 11a,b that predict $K \sim {K_0}^2$ at low concentrations and $K \sim K_0$ at high c. Figure 6 also shows a decreasing difference between salts as the salt concentration approaches the high limit of 0.1 M, which is probably an indication of the proximity to the crossover concentration $X/2K_0$, at which the fixed charge equals the invading salt, but may also indicate some variation of K_0 with ionic strength.

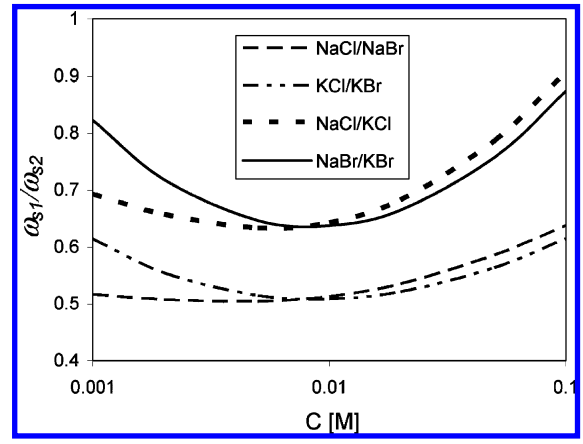

Figure 6. Ratios of the permeabilities ω_s of salts with a common ion.

The already mentioned puzzling feature of the plots in Figures 4 and 6 is the change of the trend in the low c range, in which the differences between the salts diminish or stay nearly constant and the decrease of ω_s slows down, as c approaches the lowest feed concentration 0.001 M. This observation, directly made from the $\omega_s(c)$ plots, demonstrates the advantages of the present analysis. It would have been much harder to reveal by conventional modeling, since no presently used model contains this feature. Indeed, eq 10, a simplified generic version of exclusion models used in all recently used models of NF, predicts a linear increase of ω_s at low c, as long as the single salt remains the only electrolyte in solution. In fact, if one considers the fact that K_0 should somewhat increase with concentration, as characteristic of dielectric exclusion,[53] the actual increase of ω_s with c should be even steeper than linear. This once again strongly suggests that the regular SDE picture of salt exclusion becomes inadequate even for single monovalent salts below 0.01 M. We will address this unexpected behavior in a future publication and limit the subsequent discussion to the range of 0.01−0.1 M.

3.4. Consistency of Permeabilities of Single Salts and Mixtures. The ultimate purpose of the present analysis will be to apply the obtained phenomenological coefficients for modeling of NF separations of mixed electrolytes. The "mixing rules", i.e., whether and how the coefficients measured for single salts have to be modified for salt mixtures, are an open question at present. Here we only would like to examine its consistency with the measured permeabilities for NaCl and NaBr as single salts and their equimolar mixtures within the simplified Donnan−non-Donnan model.

For the case where the fixed charge largely exceeds all invading co-ions, corresponding to the concentrations used here, a generalized analogue of eq 11b for ion i in a mixture of *monovalent* ions is easily shown to be

$$K_i \approx \frac{k_i}{X}\sum_j k_j' c_j' \tag{13}$$

where K_i and k_i are, respectively, the overall and non-Donnan partitioning coefficients of ion i and k' and c' are, respectively, the non-Donnan partitioning coefficients and corresponding concentrations of the ions in solution charged oppositely to ion i. For instance, if ion i is a cation, the summation is performed over all anions in solution and vice versa. The value of K_i is to be substituted to eq 10 and corresponds to the actual ionic partitioning coefficients of the ion, if it is a co-ion, or to the mobile fraction associated with the co-ions, if it is a counterion. It is to be substituted to eq 10 instead of salt partitioning coefficient K to yield the observed ionic permeabilities in a mixture.

Equation 13 suggests that the *ratio* of the permeabilities of Cl^- and Br^- *in a mixture* of NaCl and NaBr should be similar to the *ratio* of the permeabilities of chloride and bromide of the same cation as *single salts*. Indeed, since we have seen that the parameter A is small and may be neglected, the concentration of an ion or a single salt in the permeate may be obtained from eq 6

$$c'' \approx \frac{1}{J_V}\int_{c''}^{c'} \omega(c)\,\mathrm{d}c \approx c'\frac{\omega}{J_V+\omega} \tag{14}$$

where the last approximate relation assumes a constant or properly averaged ω. The ratio of *passages* (ratio of permeate and corrected feed concentrations) of ions 1 and 2 is then approximately

$$\frac{1-R_1}{1-R_2} = \frac{c_1''/c_1'}{c_2''/c_2'} \approx \frac{\omega_1}{\omega_2}\frac{J_V+\omega_2}{J_V+\omega_1} \tag{15}$$

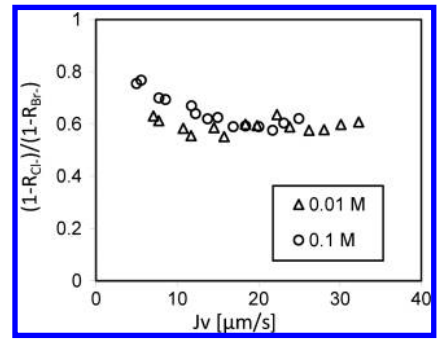

Figure 7. Ratio of the passages of chloride and bromide for NF-200 membrane and feed solutions containing 0.01 and 0.1 M equimolar mixtures of NaBr and NaCl.

Comparison of eq 15 with eq 13 and an analogue of eq 9 for individual ions shows that for large fluxes ($J_V \gg \omega$) the ratio of passages of Cl^- and Br^- *in a mixture* should approach the ratio of ionic permeabilities $\omega_{Cl^-}/\omega_{Br^-}$. This ratio in turn should be identical to the ratio of *single salt* permeabilities $\omega_{NaCl}/\omega_{NaBr}$ or $\omega_{KCl}/\omega_{KBr}$ for similar ion concentrations. Figure 7 shows the ratio $(1 - R_{Cl^-})/(1 - R_{Br^-})$ for two equimolar feed mixtures of NaCl and NaBr of total concentrations of 0.01 and 0.1 M. (The results for NaCl/NaBr mixtures are fully described in Supporting Information—see Figure S5.) Indeed, this ratio attains a constant value of about 0.6 at large fluxes, which reasonably compares with the ratio of permeabilities of single salts $\omega_{NaCl}/\omega_{NaBr}$ and $\omega_{KCl}/\omega_{KBr}$ for these feed concentrations (Figure 6). On the other hand, for small fluxes ($J_V \ll \omega$) the ratio of passages approaches unity, in agreement with eq 15. Also, in agreement with this relation, the flux $J_V \sim \omega$, at which a constant ratio $\omega_{Cl^-}/\omega_{Br^-}$ in a mixture is attained is lower for 0.01 M solution than for 0.1 M, since ω is smaller for 0.01 M (Figure 4). It is seen therefore that the simple Donnan−non-Donnan model consistently explains single and mixed salt permeabilities above about 0.01 M, i.e., beyond the puzzling low concentration range.

4. Conclusions

Using the proposed method of analysis of NF data, we obtained two phenomenological coefficients, the constant Peclét coefficient A and the concentration-dependent diffusion permeability ω_s, for several 1:1 salts with common cations and anions. Thus obtained A and $\omega_s(c)$ could then be transparently analyzed in terms of different transport equations. This analysis showed that the parameter A was very small for the studied membrane and salts, which strongly suggests that the convection could be neglected and the phenomenological equation might be greatly simplified for practical purposes. The smallness of the A values was confirmed by calculating the effective pore radius of the membranes using the relations of hindered transport theory, which produced estimates in the range of 0.2−0.3 nm that were fairly close to independent estimates from hydraulic permeabilities.

The salt permeabilities ω_s showed similar trends for all analyzed salts, which for salt concentrations $c > 0.01$ M could be well-explained using a simple SDE model based on Donnan exclusion combined with constant non-Donnan partitioning coefficients for individual ions. In this concentration range the

model adequately explained the effect of specific cations and anions on the permeability; however an unexpected anomalous regime was obtained for $c < 0.01$ M, in which ω_s seems to approach a constant value. This particular result could have passed unnoticed in "black-box" multiparameter ENP modeling and fitting and demonstrates the advantages and transparency offered by the present approach. The differences in permeabilities of salts with a common anion or cation qualitatively agree with the trend inferred from the Born equation and indicate the importance and dominance of dielectric effects in the non-Donnan contributions.

Finally, we showed that the same model and results for single salts were consistent with the results of other mixed NaCl/NaBr feed solutions, which opens a route to modeling complex salt mixtures based on single-salt parameters derived in the proposed way.

Acknowledgment. The authors are indebted to Prof. Ora Kedem for the idea of this work and numerous discussions. Dow-Filmtec and Dr. Markus Busch are gratefully acknowledged for supplying membrane samples. This work was partly supported by grants from the European Community (Project FP6 MEDINA, EU Contract No. 036997) and from the Water Authority of Israel.

Supporting Information Available: Full results of flux and rejection measurements, concentration−polarization correction, analysis of hydrodynamic conditions, and model fitting for all salts. This information is available free of charge via the Internet at http://pubs.acs.org.

References and Notes

(1) Levenstein, R.; Hasson, D.; Semiat, R. *J. Membr. Sci.* **1996**, *116*, 77.
(2) Szymczyk, A.; Labbez, C.; Fievet, P.; Vidonne, A.; Foissy, A.; Pagetti, J. *Adv. Colloid Interface Sci.* **2003**, *103*, 77.
(3) Wang, X. L.; Tsuru, T.; Nakao, S.; Kimura, S. *J. Membr. Sci.* **1997**, *135*, 19.
(4) Afonso, M. D.; de Pinho, M. N. *J. Membr. Sci.* **2000**, *179*, 137.
(5) Hagmeyer, G.; Gimbel, R. *Desalination* **1998**, *117*, 247.
(6) Lefebvre, X.; Palmeri, J.; David, P. *J. Phys. Chem. B* **2004**, *108*, 16811.
(7) Fievet, P.; Labbez, C.; Szymczyk, A.; Vidonne, A.; Foissy, A.; Pagetti, J. *Chem. Eng. Sci.* **2002**, *57*, 2921.
(8) Lanteri, Y.; Szymczyk, A.; Fievet, P. *J. Phys. Chem. B* **2009**, *120*, 57.
(9) Lefebvre, X.; Palmeri, J. *J. Phys. Chem. B* **2005**, *109*, 5525.
(10) Spiegler, K. S.; Kedem, O. *Desalination* **1966**, *1*, 311.
(11) Bungay, P. M.; Brenner, H. *J. Fluid Mech.* **1973**, *60*, 81.
(12) Deen, W. M. *AIChE J.* **1987**, *33*, 1409.
(13) Lanteri, Y.; Fievet, P.; Szymczyk, A. *J. Colloid Interface Sci.* **2009**, *331*, 148.
(14) Bruni, L.; Bandini, S. *J. Membr. Sci.* **2008**, *308*, 136.
(15) Bason, S.; Oren, Y.; Freger, V. *J. Membr. Sci.* **2007**, *302*, 10.
(16) Cahill, D. G.; Freger, V.; Kwak, S. Y. *MRS Bull.* **2008**, *33*, 27.
(17) Kedem, O.; Freger, V. *J. Membr. Sci.* **2008**, *310*, 586.
(18) Bason, S.; Kedem, O.; Freger, V. *J. Membr. Sci.* **2009**, *326*, 197.
(19) Yaroshchuk, A. E. *J. Membr. Sci.* **2002**, *198*, 285.
(20) Ben-David, A.; Bason, S.; Jopp, J.; Oren, Y.; Freger, V. *J. Membr. Sci.* **2006**, *281*, 480.
(21) www.dow.com.
(22) Bowen, W. R.; Mukhtar, H. *J. Membr. Sci.* **1996**, *112*, 263.
(23) Bowen, W. R.; Welfoot, J. S. *Chem. Eng. Sci.* **2002**, *57*, 1121.
(24) Hagmeyer, G.; Gimbel, R. *Sep. Purif. Tech.* **1999**, *15*, 19.
(25) Levich, V. G. *Physicochemical Hydrodynamics*; Prentice Hall: Upper Saddle River, NJ, 1962.
(26) Flinn, J. E. *Membrane Science and Technology*; Plenum Press: New York, 1970.
(27) Bason, S.; Freger, V. Manuscript in preparation.
(28) Freger, V. *Environ. Sci. Technol.* **2004**, *38*, 3168.
(29) Yaroshchuk, A. E. *J. Membr. Sci.* **2000**, *167*, 149.
(30) Yaroshchuk, A.; Martinez-Llado, X.; Llenas, L.; Rovira, M.; de Pablo, J.; Flores, J.; Rubio, P. *Desalin. Water Treat.* **2009**, *6*, 48.
(31) Schwartz, L. M.; Martys, N.; Bentz, D. P.; Garboczi, E. J.; Torquato, S. *Phys. Rev. E* **1993**, *48*, 4584.
(32) Torquato, S. *Random Heterogeneous Materials: Microstructure and Macroscopic Properties*; Springer-Verlag: New York, 2002.
(33) Bowen, W. R.; Mohammad, A. W.; Hilal, N. *J. Membr. Sci.* **1997**, *126*, 91.
(34) Blum, F. D.; Pickup, S.; Foster, K. R. *J. Colloid Interface Sci.* **1986**, *113*, 336.
(35) Freger, V.; Korin, E.; Wisniak, J.; Korngold, E.; Ise, M.; Kreuer, K. D. *J. Membr. Sci.* **1999**, *160*, 213.
(36) Meares, P. *Philos. Trans. R. Soc. London, B* **1977**, *278*, 113.
(37) Muhr, A. H.; Blanshard, J. M. V. *Polymer* **1982**, *23*, 1012.
(38) Raviv, U.; Giasson, S.; Frey, J.; Klein, J. *J. Phys.: Condens. Matter* **2002**, *14*, 9275.
(39) Raviv, U.; Laurat, P.; Klein, J. *Nature (London)* **2001**, *413*, 51.
(40) Torquato, S. *Rev. Chem. Eng.* **1987**, *4*, 151.
(41) Sundet, S. A. *J. Membr. Sci.* **1993**, *76*, 175.
(42) Freger, V. *Langmuir* **2005**, *21*, 1884.
(43) Freger, V. *Langmuir* **2003**, *19*, 4791.
(44) Feng, S.; Halperin, B. I.; Sen, P. N. *Phys. Rev. B* **1987**, *35*, 1987.
(45) Cotton, F. A.; Wilkinson, G. *Advanced Inorganic Chemistry*; John Wiley & Sons: New York, 1980.
(46) Babu, C. S.; Lim, C. *Chem. Phys. Lett.* **1999**, *310*, 225.
(47) *CRC Handbook of Chemistry and Physics*, 84th ed.; Lide, D. R., Ed.; CRC Press: Boca Raton, FL, 2003.
(48) Ballet, G. T.; Hafiane, A.; Dhahbi, M. *J. Membr. Sci.* **2007**, *290*, 164.
(49) Cuartas-Uribe, B.; Vincent-Vela, M. C.; Alvarez-Blanco, S.; Alcaina-Miranda, M. I.; Soriano-Costa, E. *Sep. Purif. Tech.* **2007**, *56*, 38.
(50) Ben-David, A.; Oren, Y.; Freger, V. *Environ. Sci. Technol.* **2006**, *40*, 7023.
(51) Yaroshchuk, A.; Karpenko, L.; Ribitsch, V. *J. Phys. Chem. B* **2005**, *109*, 7834.
(52) Szymczyk, A.; Fatin-Rouge, N.; Fievet, P.; Ramseyer, C.; Vidonne, A. *J. Membr. Sci.* **2007**, *287*, 102.
(53) Yaroshchuk, A. E. *Adv. Colloid Interface Sci.* **2000**, *85*, 193.

JP911615N